http://dx.doi.org/10.5012/bkcs.2014.35.11.3319

Doping-Concentration and Annealing Effects on Photoluminescence Profile of Eu(III)-doped CeO_2 nanorods

Juheon Lee, Yohan Park, Sang Woo Joo,† and Youngku Sohn*

*Department of Chemistry, Yeungnam University, Gyeongsan 712-749, Korea. *E-mail: youngkusohn@ynu.ac.kr*
†School of Mechanical Engineering, Yeungnam University, Gyeongsan 712-749, Korea
Received July 5, 2014, Accepted July 29, 2014

Eu(III)-doped CeO_2 nanorods were prepared by a co-precipitation method at room temperature, and their photoluminescence profiles were examined with different Eu(III)-doping concentrations and thermal annealing temperatures. Scanning electron microscopy, X-ray diffraction crystallography and UV-Vis absorption spectroscopy were employed to examine the morphology, crystal structure and photon absorption profiles of the nanorods, respectively. Additionally, their 2D and 3D-photoluminescence profile maps were obtained to fully understand the photoluminescence mechanism. We found that the magnetic dipole $^5D_0 \rightarrow {}^7F_1$ and the electric dipole $^5D_0 \rightarrow {}^7F_2$ transitions of Eu(III) were highly dependent on the doping concentration, annealing temperature and excitation wavelength, which was explained by the presence of different Eu(III)-doping sites (with and without an inversion center) in the CeO_2 host with a cubic crystal structure.

Key Words : Eu(III), CeO_2, Photoluminescence map, Annealing, Doping

Introduction

Extensive studies focusing on synthesis of luminescent materials, development of host materials and examination of luminescence mechanisms have been conducted in attempts to develop ideal luminescent materials.[1-7] Phosphor materials play an indispensable role in lightening and color displays. It is well known that luminescence color and efficiency are highly dependent on many factors, including crystal structure, morphology, impurity, defects, nature of the host matrix, and doping sites of the activator ion. Many efforts have been devoted to achieve ideal phosphor material which could be obtained by a good oxide support material, optimum activator doping level and crystallinity *etc.* Understanding photoluminescence occurring by host-guest charge transfer is also very important. Many different methods (*e.g.*, hydrothermal, sol-gel, electrochemical deposition, thermolysis and sonochemical methods) have been employed to modify the morphology of host materials.[8-12] Host materials play a significantly role in energy absorption and transfer to guest ions, which consequently determines the luminescence efficiency.[6,7] An electrochemical deposition method was used to synthesize Eu(III)-doped CeO_2 nanobelts by Wang *et al.*[13] Additionally, Deus *et al.* employed a microwave hydrothermal method to synthesize CeO_2 nanospheres and examine growth of the nanocrystals with different mineralizer agents.[11] Ansari *et al.* prepared CeO_2:Ln^{3+} films by dip-coating a precursor solution followed by thermal annealing.[14] CeO_2 has been used as a model host material because it has a cubic crystal structure with convertible oxidation states (Ce^{4+}/Ce^{3+}) and provides a guest activator with two different doping sites with and without an inversion center. Eu(III) has been extensively used as an activator ion for red emitting phosphor materials.[1-7,15-30] In such materials, the host absorbs incident light to transfer its energy to the Eu(III) activator. The luminescence from Eu(III) is associated with $^5D_0 \rightarrow {}^7F_J$ (J = 0, 1, 2, 3, 4) transitions, and the hypersensitive $^5D_0 \rightarrow {}^7F_2$ transition determines the red color.[6,7] Sohn previously synthesized Eu(III)-doped CeO_2 nanoparticles using a hydrothermal method (at 120 °C) and then examined their photoluminescence profiles for 1 and 10 mol % Eu(III)-doped samples.[29]

In this study, we investigated the photoluminescence of Eu(III)-doped CeO_2 nanorods by employing a 2D and 3D-photoluminescence profile mapping.[27-30] This is the first report of Eu(III)-doped CeO_2 nanorods prepared at room temperature using various doping concentrations and thermal annealing temperatures. A thorough understanding of the relationship between photoluminescence and doping-concentrations of activator ions and thermal annealing is essential to identification of methods for development of efficient luminescent materials.

Experimental

To synthesize CeO_2 nanowires, we mixed 10.0 mL 0.1 M Ce(III) nitrate hexahydrate and 20.0 mL Millipore water, added 2.0 mL of ammonia (~30%) solution, and placed the mixed solution in a Teflon bottle at room temperature for 15 hours until precipitates settled completely and a colloidal layer (with ultramarine color) was fully formed. The final products were fully washed with deionized water and ethanol, then dried in a vacuum oven at room temperature for one week. For doping Eu(III) activator ions of 0.1, 1 and 10 mol %, we mixed an appropriate amount of 0.1 M Eu(III) nitrate solutions into the mother solution before adding ammonia, and the rest of the experimental procedure was same. We annealed the prepared samples at temperatures of

400, 600 and 800 °C for 4 h under ambient air. The crystal structure was determined by examining the X-ray diffraction (XRD) patterns taken using a PANalytical X'Pert Pro MPD powder diffractometer with Cu Kα radiation. The surface morphology of the sample was examined by transmission electron microscopy (TEM, Hitachi HE-600). Diffuse reflectance absorption spectra were taken using a SCINCO NeoSys-2000 double beam UV–Vis spectrophotometer. A SCINCO FluoroMate FS-2 was used to obtain 2D and 3D-photoluminescence profile map and the corresponding excitation/emission spectra. The PL instrument collects all emission spectra at a selected excitation wavelength region, and then the software converts the data to the 2D and 3D-photoluminescence (PL) contour map.

Results and Discussion

Figure 1 shows typical powder X-ray diffraction patterns of as-prepared and 800 °C-annealed Eu(III)-doped (10 mol %) CeO_2 nanorod powder samples. The sizes of the nanorods were estimated to be about 5-10 nm wide and 50-100 nm long based on the TEM image (Figure 1). For the as-prepared sample, the XRD peaks were broad and in good accordance with the XRD patterns of cubic (Fm-3m) (JCPDS 03-065-5923) CeO_2. The peak positions at around 2Θ = 28.4, 33.1, 47.4, 56.3, 59.0, and 69.4° were assigned to the (111), (200), (220), (311), (222), and (400) planes, respectively. No other peaks were found, indicating homogeneous doping of Eu(III) into the CeO_2 host material. Upon annealing, the XRD became much narrower with no substantial change in peak position due to an increase in crystallinity, which is consistent with the results of previous studies.[6]

Figure 2 shows the UV-visible absorption spectra of undoped CeO_2 and 10 mol % Eu(III)-doped nanorod samples before and after 800 °C-thermal annealing. The Y-axis absorbance was converted from the diffuse reflectance data by the Kubelka-Munk method. The inset of Figure 2 re-plots the spectra $(\alpha h\nu)^2$ versus photon energy (hν), where α is the absorption coefficient. The spectra of the as-prepared samples were exactly superimposible. The band gap edge of the

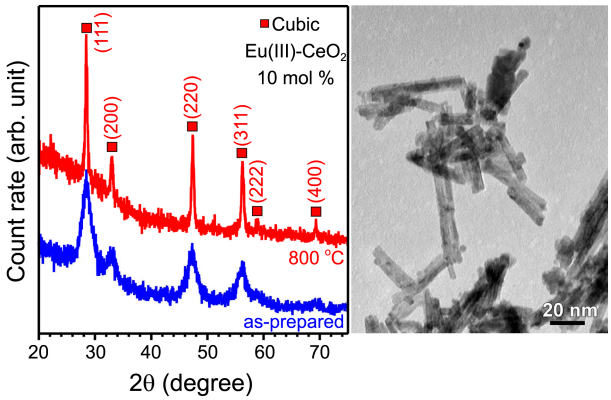

Figure 1. Typical powder X-ray diffraction patterns (left) of as-prepared and 800 °C-annealed Eu(III)-doped (10 mol %) CeO_2 nanorod powder samples, and a typical TEM image (right).

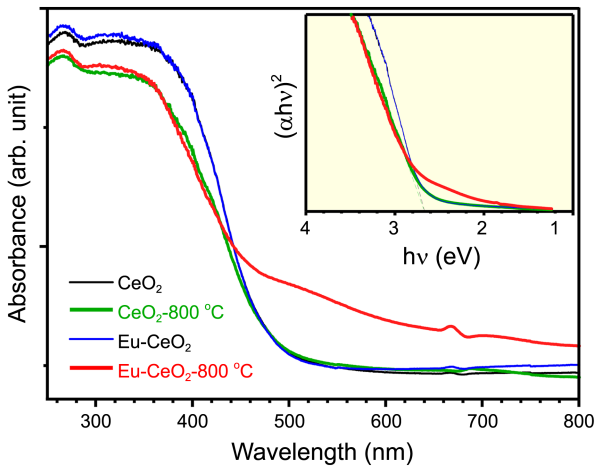

Figure 2. Diffuse reflectance UV-Visible absorption spectra of as-prepared and 800 °C-annealed Eu(III)-doped (10 mol %) CeO_2 nanorod powder samples compared with those of undoped CeO_2. The inset shows the plots of $(\alpha h\nu)^2$ versus photon energy (hν) for the corresponding samples.

nanorods was measured to be ~2.7 eV, which was lower than that reported in previous studies.[5,14] Malleshappa *et al.* observed direct band gaps of 3.20 to 3.40 eV for Tb(III)-doped CeO_2 (with 5-9 nm size) nanoparticles prepared by a low temperature solution combustion method.[5] Ansari *et al.* reported a band gap of 3.57 eV for a CeO_2:Tb^{3+} film prepared using a sol-gel and dip-coating technique.[14] The broad absorption below 400 nm was attributed to O^{2-} (2p) – Ce^{4+} (4f) charge transfer.[5,6] No noticeable direct absorption peaks corresponding to Eu(III) were found. Upon annealing at 800 °C the charge transfer band decreased somewhat, while the absorption edge of the undoped CeO_2 showed no significant change. However, for the 10 mol % Eu(III)-doped sample, the absorption in the visible region clearly increased upon thermal annealing due to Eu doping effect.

Before discussing the extensive PL results, to help readers better understand we summarized experimental results and purposes in Table 1.

Figure 3 shows 2D-PL profile maps of as-prepared and annealed (400, 600 and 800 °C) Eu(III)-doped CeO_2 nanorod powder samples prepared using various doping concentrations (0, 0.1, 1 and 10 mol %). The corresponding 3D-PL

Table 1. Summarized experimental results and purposes

Experiments	Purposes
PL for CeO_2 doped with different concentrations (0, 0.1, 1 and 10 mol %) of Eu(III) activator ions	Examine PL intensity and doped sites with doped concentrations
PL for CeO_2 annealed at different (400, 600 and 800 °C) temperatures	Examine crystallinity (and quenching species) effects on PL and color purity
PL taken at direct (395 and 465 nm) and indirect (300 and 350 nm) excitation wavelengths	Examine host (CeO_2)-guest (Eu) charge transfer and doping site effects on PL and color purity

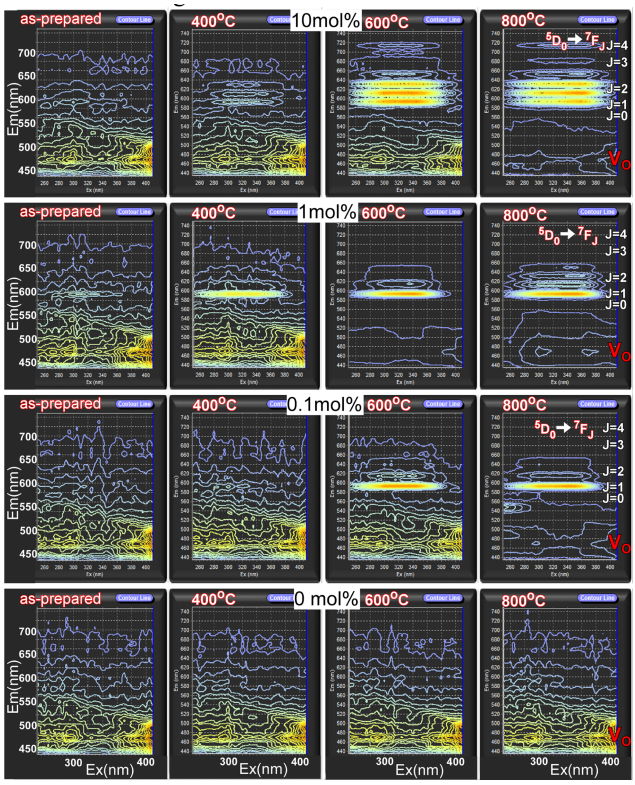

Figure 3. 2D-PL profile map of as-prepared and annealed (400, 600 and 800 °C) Eu(III)-doped CeO_2 nanorod powder samples with various doping concentrations (0, 0.1, 1 and 10 mol %). Ex (nm) range is from 250 to 405 nm, and Em (nm) range is from 440 to 750 nm.

profile maps were provided in Supporting Information, Figure S1. The results revealed that the PL profile was highly doping-concentration and annealing temperature dependent. The densely spaced region indicates a stronger signal and becomes much clearer for the annealed samples. For the 0.1 and 1 mol % Eu(III)-doped samples, one densely spaced region emerged. For the 10 mol % Eu(III)-doped sample, three densely spaced regions newly appeared after thermal annealing at 600 and 800 °C.

Figure 4 displays emission spectra of as-prepared and annealed (400, 600 and 800 °C) Eu(III)-doped CeO_2 nanorod powder samples prepared using various doping concentrations (0, 0.1, 1 and 10 mol %) at an excitation wavelength of λ_{ex} = 395 nm. The wavelength of 395 nm corresponds to the direct $^5L_6 \leftarrow {}^7F_0$ of Eu(III), which is the most commonly used for direct f-f excitation of Eu(III). For the emission spectra recorded from 450 to 740 nm, a broad peak was commonly found at 470 nm. This has commonly been attributed to oxygen defects, which are often present in oxide materials. This peak actually consists of several peaks (452, 469, 483 and 495 nm), possibly due to oxygen defect sites with various charge states.[29-31] At low doping concentrations (0 and 0.1 mol %), the broad peak showed a slight change with annealing temperature. However, the band was significantly altered at high (1 and 10 mol %) doping concentrations. The large variation with annealing temperature was likely due to charge unbalance and size mismatch between host Ce^{4+} and guest Eu(III).[6] For the 10 mol % Eu(III)-doped sample, the intensity became much weaker upon annealing at 400 or 800 °C. The band showed a large decrease in intensity upon annealing at 400 °C, while the intensity increased upon further annealing at 600 and 800 °C. The 400 °C-annealed samples commonly showed the weakest intensity.

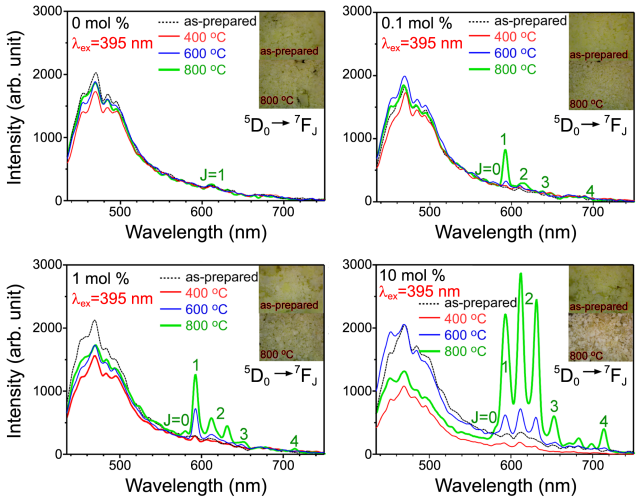

Figure 4. Emission (λ_{ex} = 395 nm) spectra of as-prepared and annealed (400, 600 and 800 °C) Eu(III)-doped CeO_2 nanorod powder samples with various doping concentrations (0, 0.1, 1 and 10 mol %). The insets show optical microscopy images of the corresponding powder samples before and after annealing at 800 °C.

Sharp emission peaks were found between 560 and 750 nm (Figure 4), and these changed remarkably with doping concentration and annealing temperature. The emission peaks in this region were associated with $^5D_0 \rightarrow {}^7F_J$ (J = 0–4) transitions of Eu(III) ions. For the as-prepared samples, no significant emission peaks were found in this region, while the $^5D_0 \rightarrow {}^7F_J$ (**J** = 0 – 4) transition peaks were found to be very weak for the 10 mol % Eu(III)-doped sample. Upon annealing at 400 °C, no significant increase in peak intensity was observed between 560 and 750 nm, while the broad band showed a significant change. Strong $^5D_0 \rightarrow {}^7F_J$ (J = 0–4) emission peaks were reported for Eu(III)-doped CeO_2 nanoparticles prepared by a hydrothermal method,[29] which is inconsistent with the results of the present study. These findings indicate that luminescence efficiency is strongly dependent on preparation method. Upon annealing of the Eu(III)-doped samples at 600 °C, sharp emission peaks clearly and newly appeared, while undoped CeO_2 showed no new peaks. The intensities increased linearly with increasing doping concentration. As shown in the inset photo, the 10 mol % Eu(III)-doped powder sample appeared pale red upon annealing at 800 °C (Figure 4). When annealing was conducted at 800 °C, the sharp emission peaks was enhanced significantly. For the 10 mol % Eu(III)-doped sample, the following $^5D_0 \rightarrow {}^7F_J$ (J = 0–4) emission peaks were dominant: $^5D_0 \rightarrow {}^7F_0$ (580 nm), $^5D_0 \rightarrow {}^7F_1$ (590 nm), $^5D_0 \rightarrow {}^7F_2$ (611 and

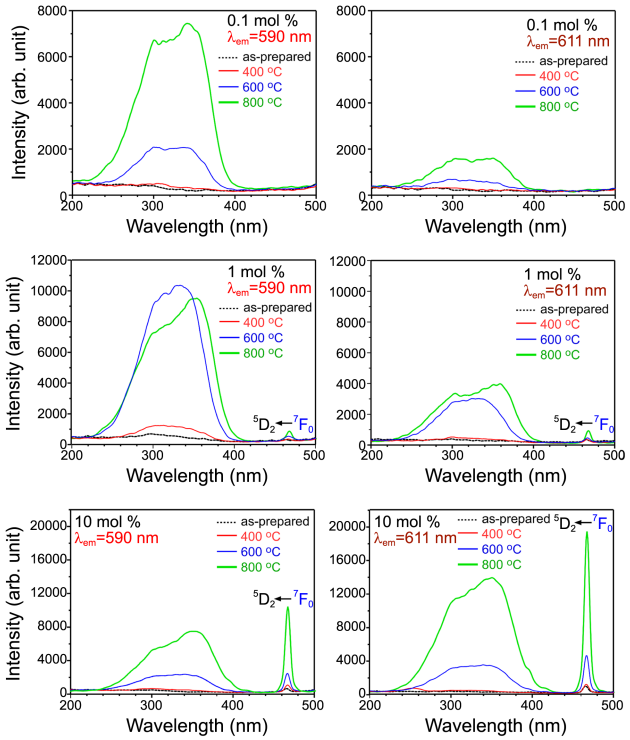

Figure 5. Excitation (λ_{em} = 590 and 611 nm) spectra of as-prepared and annealed (400, 600 and 800 °C) Eu(III)-doped CeO_2 nanorod powder samples with various doping concentrations (0.1, 1 and 10 mol %).

631 nm), $^5D_0 \rightarrow {}^7F_3$ (653 nm), and $^5D_0 \rightarrow {}^7F_4$ (683, 699, and 714 nm). For the 1 mol % Eu(III)-doped sample, we found $^5D_0 \rightarrow {}^7F_0$ (580 nm), $^5D_0 \rightarrow {}^7F_1$ (590 nm), $^5D_0 \rightarrow {}^7F_2$ (611 and 631 nm), $^5D_0 \rightarrow {}^7F_3$ (652 nm), and $^5D_0 \rightarrow {}^7F_4$ (714 nm) transition peaks. The 0.1 mol % Eu(III)-doped sample showed $^5D_0 \rightarrow {}^7F_1$ (590 nm) and $^5D_0 \rightarrow {}^7F_2$ (611 nm) peaks. Since we used the direct $^5L_6 \leftarrow {}^7F_0$ transition wavelength (λ_{ex} = 395 nm) of Eu(III), the intensity increased with increasing doping concentrations, as expected.

However, the luminescence profiles were critically different with doping concentrations. Specifically, the $^5D_0 \rightarrow {}^7F_1$ (590 nm) transition was dominant relative to the $^5D_0 \rightarrow {}^7F_2$ (611 nm) transition at low (0.1 and 1 mol %) doping concentrations. Moreover, the emission intensity ratios of ($^5D_0 \rightarrow {}^7F_1$)/($^5D_0 \rightarrow {}^7F_2$) were found to be 5.23, 2.79 and 0.76 for 0.1, 1 and 10 mol % Eu(III)-doped samples, respectively. The ratio showed the largest value at the lowest doping concentration. It is well known that the $^5D_0 \rightarrow {}^7F_2$ transition is electric dipole allowed and sensitive to a structural environment, while the $^5D_0 \rightarrow {}^7F_1$ transition is magnetic dipole allowed and insensitive to the environment. Since the electric dipole transition is forbidden when Eu(III) is doped at a site with an inversion center, we concluded that Eu(III) became doped at less symmetric sites as the doping concentration increased.[6,7] This phenomenon is discussed in detail below.

We selected two different emission peaks of 590 (magnetic dipole $^5D_0 \rightarrow {}^7F_1$) and 611 nm (electric dipole $^5D_0 \rightarrow {}^7F_1$) and took excitation spectra of Eu(III)-doped samples annealed at different temperatures. Figure 5 displays the excitation spectra of as-prepared and annealed (400, 600 and 800 °C) Eu(III)-doped CeO_2 nanorods prepared with various doping concentrations (0.1, 1 and 10 mol %) taken at fixed emission wavelengths of 590 and 611 nm. For the as-prepared and 400 °C-annealed samples, the bands below 400 nm were extremely weak. For the 0.1 and 1 mol % Eu(III)-doped samples, the intensity of the bands increased slightly upon 400 °C annealing. A weak peak was also observed at 465 nm for the 10 mol % Eu(III)-doped samples, which was attributed to the direct $^5D_2 \leftarrow {}^7F_0$ transition of Eu(III). The direct $^5L_6 \leftarrow {}^7F_0$ transition peak at 395 nm was not distinguished from the strong band at below 400 nm. Upon annealing at 600 °C, the broad band increased greatly, and two broad peaks were commonly found at around 300 and 350 nm. The peak at 465 nm became stronger for the 10 mol % Eu(III)-doped sample, and was dominant after annealing at 800 °C. Upon annealing at 800 °C, the intensities of the two bands became much more stronger for the 0.1 and 10 mol % Eu(III)-doped samples at λ_{em} = 590 and 611 nm. The increase in intensity upon annealing was due to the decrease in quenching sites and increase in crystallinity.[23] The peak positions of the bands showed no significant change with annealing temperature. Interestingly, for the 1 mol % Eu(III)-doped sample, the bands became slightly weaker at λ_{em} = 590 nm, while they became somewhat stronger after 800 °C annealing. Moreover, the band at 300 nm showed no change in position, while the other band was red-shifted by 20 nm from 330 nm to 350 nm. The bands at λ_{em} = 590 nm were stronger than those at λ_{em} = 611 nm for the 0.1 and 1 mol % Eu(III)-doped samples. However, for the highly doped (10 mol %) sample, the bands at λ_{em} = 611 nm were stronger than those at λ_{em} = 590 nm. The peak (direct $^5D_2 \leftarrow {}^7F_0$ transition) at 465 nm was dominant in the 800 °C-annealed 10 mol % Eu(III)-doped sample. The broad band below 400 nm has been attributed to a charge transfer from O^{2-} to Ce(IV).[6,7,16] The bands at 300 and 340 nm were attributed to surface and bulk sites of CeO_2, respectively.[6] Tiseanu *et al.* prepared Eu(III)-impregnated CeO_2 nanocrystals and found no charge transfer band; however, they observed a strong asymmetric band at 340 nm upon annealing to 500 °C,[6] with no peak around 300 nm. In their study, the band was found to be red-shifted from 340 nm to 370 nm after thermal annealing to 1000 °C, which is consistent with the present study. They attributed the shift to an energy gap dependent on annealing temperature (or crystallinity). Since the Eu-O charge transfer band is also located at around 300 nm,[4] efficient energy transfer from host Ce(IV) to guest Eu(III) will be expected. For Eu(III)-CeO_2 nanoparticles prepared by a hydrothermal method, Sohn observed a predominant charge transfer band at 350 nm, with a weak shoulder peak at 300 nm.[29] Li *et al.* investigated charge transfer bands of bulk and nano materials and found that nano-materials showed dominant peaks at shorter wavelengths.[32] For $Sr_{1.7}Eu_{0.3}M_{0.3}CeO_{4.3}$ ($M = Li^+$, Na^+, K^+) samples, Shi *et al.* found that the intensity of the charge

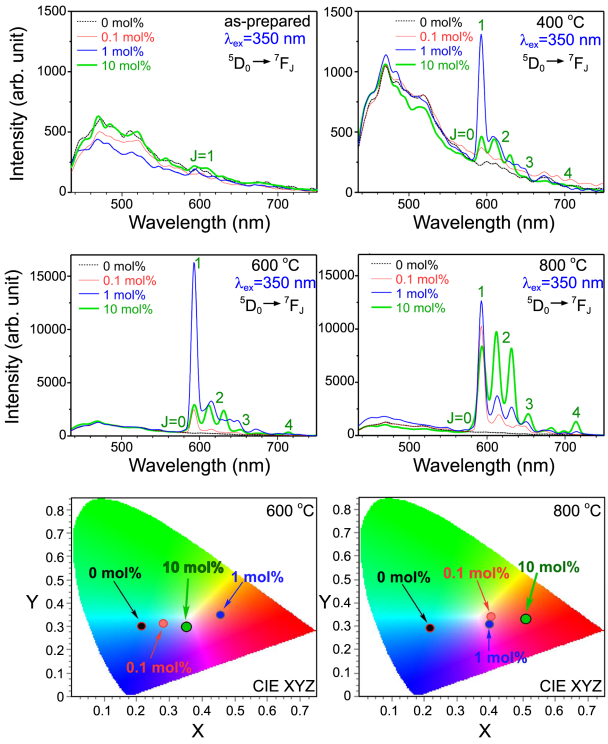

Figure 6. Emission (λ_{ex} = 350 nm) spectra of as-prepared and annealed (400, 600 and 800 °C) Eu(III)-doped CeO_2 nanorods with various doping concentrations (0, 0.1, 1 and 10 mol %), and the corresponding CIE xyz color coordinates with various doping concentrations for 600 and 800 °C annealed Eu(III)-doped CeO_2 nanorods.

transfer band at 350 nm was dependent on the alkali metals as follows: $Li^+ > Na^+ > K^+$.[4] However, they found that the band at 300 nm showed no significant change with alkali metals. In the present study, the charge transfer band (at 300 nm) of the surface site of the nanorods showed a comparable intensity to that (at 350 nm) of the bulk site.

To examine the photoluminescence profile under an excitation wavelength (referred to as indirect excitation) of the charge transfer band, we recorded emission spectra of as-prepared and annealed (400, 600 and 800 °C) Eu(III)-doped CeO_2 nanorods generated using various doping concentrations (0, 0.1, 1 and 10 mol %) at excitation wavelengths of 300 (Supporting Information, Fig. S2) and 350 nm (Figure 6). The photoluminescence profiles at λ_{ex} = 300 nm were very similar those at λ_{ex} = 350 nm, which could have been due to a similar origin of the charge transfer bands at 300 and 350 nm. As a result, similar photoluminescence profiles were sensitized by the charge transfer absorption. Because of this similarity, we only included the discussion of the photoluminescence profiles at λ_{ex} = 350 nm in Figure 6.

At an excitation wavelength of 350 nm, the as-prepared sample showed a broad peak at 470 nm, which was attributed to oxygen defects created in the oxide support. Upon annealing at 400 °C, several peaks newly appeared between 580 and 750 nm. The emission was attributed to $^5D_0 \rightarrow {}^7F_J$ (J = 0, 1, 2, 3, and 4) transitions. The 1 mol % Eu(III)-doped sample showed the highest peak intensity at 590 nm, which

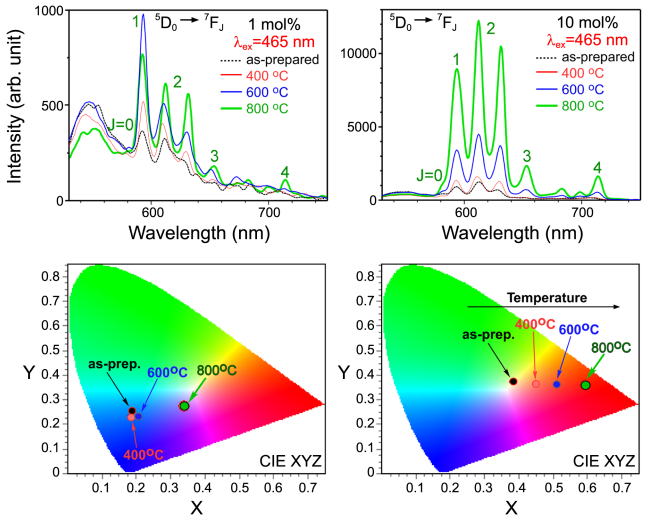

Figure 7. Emission (λ_{ex} = 465 nm) spectra of as-prepared and annealed (400, 600 and 800 °C) Eu(III)-doped CeO_2 nanorods with doping concentrations of 1 (top left) and 10 mol % (top right), and the corresponding CIE xyz color coordinates with annealing temperatures.

was comparable to that of the broad band. The dominant peak at 590 nm was attributed to the magnetic dipole allowed $^5D_0 \rightarrow {}^7F_1$ transition, which is insensitive to the local chemical environment.[6,7] For the 10 mol % Eu(III)-doped sample, the peak at 590 nm decreased dramatically by 80%. The intensity ratios of ($^5D_0 \rightarrow {}^7F_1$)/($^5D_0 \rightarrow {}^7F_2$) were found to be 4.15 and 1.0 for the 400 °C-annealed 1 and 10 mol % Eu(III)-doped samples, respectively. Upon annealing at 600 °C, the peaks at 590 nm were increased by 15× and 11× for the 1 and 10 mol % Eu(III)-doped samples, respectively. The intensity of the ($^5D_0 \rightarrow {}^7F_1$)/($^5D_0 \rightarrow {}^7F_2$) ratio increased from 4.15 to 5.34 for the 600 °C-annealed 1 mol % Eu(III)-doped sample, while it remained constant at 1.0 for the 10 mol % Eu(III)-doped sample. For the 0.1 mol % Eu(III)-doped sample, the peak at 590 nm also clearly appeared, and was stronger than the peak at 611nm, with a ($^5D_0 \rightarrow {}^7F_1$)/($^5D_0 \rightarrow {}^7F_2$) ratio of 5.46. Upon annealing at 800 °C, the photoluminescence profiles changed more dramatically. For the 800 °C-annealed 0.1 mol % Eu(III)-doped sample, the peak ($^5D_0 \rightarrow {}^7F_1$) at 590 nm increased by 4.8×. For the 10 mol % Eu(III)-doped sample, the peaks at 590 and 611 nm increased by 3.2× and 3.7×, respectively. However, for the 1 mol % Eu(III)-doped sample, the peak at 590 nm decreased by 24%, while the peak at 611 nm increased somewhat by 1.2. The intensity ratios of ($^5D_0 \rightarrow {}^7F_1$)/($^5D_0 \rightarrow {}^7F_2$) were observed to be 5.9, 3.5 and 0.85 for the 800 °C-annealed 0.1, 1 and 10 mol % Eu(III)-doped samples, respectively.

As discussed above, the intensity ratio of $(^5D_0 \rightarrow {}^7F_1)_{590nm}$/$(^5D_0 \rightarrow {}^7F_2)_{611nm}$ was larger at a lower doping concentration. In other words, the peak at 590 nm was stronger than the peak at 611 nm. When Eu(III) is doped at an octahedral site in the CeO_2 host, the localized symmetry of Eu(III) may or may not have an inversion center depending on the adjacent ions. The $^5D_0 \rightarrow {}^7F_2$ transition is electric dipole allowed, but forbidden when the Eu(III) activator has the local site sym-

metry with an inversion center. When the activator has lower site symmetry without an inversion center, the transition is allowed to show a luminescence peak. The magnetic dipole $^5D_0 \rightarrow {}^7F_1$ transition is insensitive to local site symmetry. It is assumed that, at low doping concentrations, Eu(III) is doped at a higher symmetry site with an inversion center. As the doping concentration increases, Eu(III) with a lower site symmetry will be increased.[7,24,29] As a result, the probability of a $^5D_0 \rightarrow {}^7F_2$ transition is increased to show a stronger luminescence peak, as occurred in the present study. Based on these results, it was also concluded that the energy transfer occurs more efficiently from the CeO_2 host to Eu(III) guests with high symmetry than to Eu(III) guests with low symmetry. This is not surprising because a good wave function mixing state transfers energy more efficiently. The corresponding Commission Internationale Del'Eclairage (CIE) color coordinates are displayed in Figure 6. For the undoped CeO_2, the CIE coordinate was in the blue region and showed no critical change with annealing temperature. However, the CIE coordinates for the 0.1 and 10 mol % Eu(III)-doped samples were shifted to the reddish region. Under 350 nm excitation, the 10 mol % Eu(III)-doped sample prepared by 800 °C annealing showed the highest red quality. This was attributed to an increase in $^5D_0 \rightarrow {}^7F_2$ emission by increasing crystallinity. For the 600 °C-annealed 1 mol % Eu(III)-doped sample, the CIE coordinate was observed in the red region. However, the coordinate was shifted to the pale red region upon annealing at 800 °C.

We further examined the photoluminescence profiles under a direct excitation wavelength. Since the direct $^5L_6 \leftarrow {}^7F_0$ transition peak at 395 nm was located in the indirect charge transfer band, we selected another direct transition ($^5D_2 \leftarrow {}^7F_0$ transition) at 465 nm to further elucidate doping-concentration and annealing temperature-dependent photoluminescence profiles. The excitation at 465 nm showed stronger (4) $^5D_0 \rightarrow {}^7F_J$ emission signals than that at 395 nm. Figure 7 shows the emission ($\lambda_{ex} = 465$ nm) spectra of as-prepared and annealed (400, 600 and 800 °C) Eu(III)-doped CeO_2 nanorods with doping concentrations of 1 and 10 mol %, as well as the corresponding CIE xyz color coordinates with annealing temperatures. For the 0.1 mol % Eu(III)-doped sample, the $^5D_0 \rightarrow {}^7F_J$ ($J = 0$–4) emission peaks were extremely weak; therefore, we did not discuss them here. For the 1 mol % Eu(III)-doped sample, the photoluminescence intensity was much weaker under a direct excitation wavelength of 465 nm than under indirect excitation wavelengths of 300 and 350 nm. However, for the 10 mol % Eu(III)-doped sample, the photoluminescence under direct excitation showed comparable intensity to that under indirect excitation. The intensity of the 10 mol % Eu(III)-doped sample was about 10× stronger than that of the 1 mol % Eu(III)-doped sample, and the intensity ratio was close to the doping-concentration ratio (10 mol %/1 mol %). The CIE xyz color coordinates of the as-prepared, 400 and 600°C-annealed 1 mol % Eu(III)-doped samples were similarly positioned in the blue region. After annealing at 800°C, the coordinates shifted to the red side due to the relative increase of $^5D_0 \rightarrow {}^7F_2$ emissions. For the 10 mol % Eu(III)-doped sample, the $^5D_0 \rightarrow {}^7F_J$ emission peaks were linearly increased with increasing temperature, which caused the CIE coordinates to shift to a deeper red region.

Conclusion

We successfully prepared CeO_2 nanorods and doped Eu(III) into their cubic crystal structure by a facial co-precipitation method conducted at room temperature. We fully examined the photoluminescence profiles of Eu(III)-doped CeO_2 nanorods generated using various doping concentrations and thermal annealing temperatures. At a low Eu(III)-doping concentration, photoluminescence was primarily sensitized by indirect charge transfer (O^{2-} to Ce^{4+} of CeO_2) excitations at 300 and 350 nm. Two charge transfer bands at 300 and 350 nm were attributed to CeO_2 at surface and bulk sites, respectively. The energy transfer from the CeO_2 host to the Eu(III) guest with high symmetry was more efficient than that with low symmetry. At a high Eu(III)-doping concentration, photoluminescence occurred *via* direct excitation of Eu(III). The direct excitation at 465 nm ($^5D_2 \leftarrow {}^7F_0$ transition) showed a much stronger (4×) photoluminescence signal than that at 395 nm ($^5L_6 \leftarrow {}^7F_0$ transition). As-prepared samples showed only broad emission at 470 nm due to oxygen defects, with no $^5D_0 \rightarrow {}^7F_J$ ($J = 0$, 1, 2, 3, 4) transition signals from the Eu(III) guests. The $^5D_0 \rightarrow {}^7F_J$ emission increased dramatically with increasing thermal annealing temperature due to the increase in crystallinity and decrease in quenching sites. At low doping concentration, the magnetic dipole $^5D_0 \rightarrow {}^7F_1$ emission transition at 590 nm was dominant, while at high doping concentration the electric dipole $^5D_0 \rightarrow {}^7F_2$ emission transition at 611 nm showed a comparable intensity. These findings confirm that, at low doping concentration, Eu(III) is more likely positioned at the octahedral site with an inversion center. At high doping concentration, Eu(III) is also positioned at less symmetric sites without an inversion center. Overall, this is the first study to fully examine the photoluminescence profiles of CeO_2 nanorods doped with Eu(III) using various doping concentrations and annealing temperatures. In addition, the 2D and 3D-photoluminescece profile mapping was useful for deeper investigation of the energy transfer and photoluminescence mechanism.

Acknowledgments. This work was supported by the 2013 Yeungnam University research grant.

References

1. Wang, Z.; Teng, X.; Li, P. *J. Alloys Compd.* **2014**, *589*, 549.
2. Zhang, D.: Yan, T.; Shi, L.; Li, H.; Chiang, J. F. *J. Alloys Compd.* **2010**, *506*, 446.
3. Fang, Y.-C.; Huang, X.-R.; Juang, Y.-D.; Chu, S.-Y. *J. Am. Ceram. Soc.* **2011**2, *95*, 1613.
4. Shi, L.; Li, C.; Su, Q. *J. Alloys Compd.* **2011**, *509*, 4209.
5. Malleshappa, J.; Nagabhushana, H.; Sharma, S.C.; Sunitha, D. V.; Dhananjaya, N.; Shivakumara, C.; Nagabhushana, B. M. *J. Alloys*

Compd. **2014**, *590*, 131.
6. Tiseanu, C.; Parvulescu, V. I.; Sanchez-Dominguez, M.; Boutonnet, M. *J. Appl. Phys*. **2012**, *112*, 013521.
7. Li, L.; Yang, H. K.; Moon, B. K.; Fu, Z.; Guo, C.; Jeong, J. H.; Yi, S. S.; Jang, K.; Lee, H. S. *J. Phys. Chem. C* **2009**, *113*, 610.
8. Dutta, D. P.; Manoj, N.; Tyagi, A. K. *J. Lumin*. **2011**, *131*, 1807.
9. Taguchi, M.; Takami, S.; Adschiri, T.; Nakane, T.; Sato, K.; Naka, T. *CrystEngComm* **2011**, *13*, 2841.
10. Meng, F.; Wang, L.; Cui, J. *J. Alloys Compd*. **2013**, *556*, 102.
11. Deus, R. C.; Cilense, M.; Foschini, C. R.; Ramirez, M. A.; Longo, E.; Simoes, A. Z. *J. Alloys Compd*. **2013**, *550*, 245.
12. Wang, G.;Mu, Q.; Chen, T.; Wang, Y. *J. Alloys Compd*. **2010**, *493*, 202.
13. Wang, Z.; Quan, Z.; Lin, J. *Inorg. Chem*. **2007**, *46*, 5237.
14. Ansari, A. A.; Singh, S. P.; Malhotra, B. D. *J. Alloys Compd*. **2011**, *509*, 262.
15. Wang, X.; Zhang, D.; Li, Y.; Tang, D.; Xiao, Y.; Liu, Y.; Huo, Q. *RSC Adv*. **2013**, *3*, 3623.
16. Zeng, L.; Chen, D.; Huang, F.; Yang, A.; Lei, L.; Wang, Y. *J. Alloys Compd.* **2012**, *534*, 64.
17. Yu, Y.; Chen, D.; Huang, P.; Lin, H.; Yang, A.; Wang, Y. *J. Alloys Compd*. **2012**, *513*, 626.
18. Shi, S.; Hossu, M.; Hall, R.; Chen, W. *J. Mater. Chem.* **2012**, *22*, 23461.
19. Kremenovic, A.; Bozanic, D. K.; Welsch, A.-M.; Jancar, B.; Nikolic, A. S.; Boskovic, M.; Colomban, Ph.; Fabian, M.; Antic, B. *J. Nanosci. Nanotech.* **2012**, *12*, 8893.
20. Kumar, A.; Babu, S.; Karakoti, A. S.; Schulte, A.; Seal, S. *Langmuir* **2009**, *25*, 10998.
21. Wang, Z.-L.; Li, G.-R.; Ou, Y.-N.; Feng, Z.-P.; Qu, D.-L.; Tong, Y.-X. *J. Phys. Chem*. *C* **2011**, *115*, 351.
22. Guo, H.; Qiao, Y. *Appl. Surf. Sci*. **2008**, *254*, 1961.
23. Babu, S.; Schulte, A.; Seal, S. *Appl. Phys. Lett*. **2008**, *92*, 123112.
24. Liu, X.; Chen, S.; Wang, X. *J. Lumin*. **2007**, *127*, 650.
25. Oikawa, M.; Fujihara, S. *J. Euro. Ceram. Soc*. **2005**, *25*, 2921.
26. Fujihara, S.; Oikawa, M. *J. Appl. Phys*. **2004**, *95*, 8002.
27. Sohn, Y. *Ceram. Inter*. **2014**, *40*, 2467.
28. Sohn, Y. *Ceram. Inter*. **2013**, *39*, 9157.
29. Sohn, Y. *J. Am. Ceram. Soc*. **2013**, *12*, 3747.
30. Cho, I.; Kang, J.-G.; Sohn, Y. *Bull. Korean Chem. Soc*. **2014**, *35*, 575.
31. Askrabic, A.; Dohcevic-Mitrovic, Z. D.; Araujo, V. D.; Ionita, G.; de Lima, M. M., Jr.; Cantarero, A. J. *J. Phys. D* **2013**, *46*, 495306.
32. Li, L.; Zhou, S.; Zhang, S. *Chem. Phys. Lett*. **2008**, *453*, 283.